ARTICLE NO. 79-0793R

Coupled Bending-Torsion Flutter in Cascades

Oddvar Bendiksen* and Peretz Friedmann†
University of California, Los Angeles, Calif.

A method is presented for determining the aeroelastic stability boundaries of a cascade with aerodynamic, inertial, and structural coupling between the bending and torsional degrees of freedom. A computer program has been written to systematically investigate the effect of this coupling on cascade stability over a wide range of design parameters. Results presented illustrate that the bending-torsion interaction has a pronounced effect on the cascade flutter boundary, despite no appreciable tendency toward frequency coalescence as flutter is approached. The analysis also indicates that bending flutter is possible even in the absence of finite mean lift.

Nomenclature

a	= location of elastic axis, nondimensional (Fig. 2)
$[A]$	= aerodynamic matrix
b	= semichord
c	$= 2b$ = chord
$[D]$	= matrix defined by Eq. (16)
$\{F\}$	= generalized force matrix defined by Eq. (4)
g	= structural damping
g_B, g_T	= structural damping in bending and torsion, respectively
h	= bending deflection (Fig. 2)
$\bar{h}$	$= h/b$ = nondimensional bending deflection
i	$= \sqrt{-1}$ or integer index
I_α	$= mr_\alpha^2 b^2$ = mass moment of inertia per unit span about the axis $x = ba$
k	$= \omega b/U$ = reduced frequency
k_T	$= \omega_T b/U$ = critical reduced frequency for single-degree-of-freedom torsional flutter (Fig. 5)
K_h, K_α	= blade bending and torsional stiffness, respectively
$[K]$	= stiffness matrix defined by Eq. (4)
$[\bar{K}_d]$	= nondimensionalized stiffness matrix with structural damping coefficients included, as defined by Eq. (13)
L	= lift, positive up, per unit span
m	= mass per unit span of blade
M	= moment about axis $x = ba$, positive clockwise, per unit span
$[M]$	= mass matrix defined by Eq. (4)
N	= number of blades in rotor
p	= exponent
$\bar{p}_R$	= real part of p, nondimensionalized [Eq. (18)]
$\{q\}$	= generalized coordinate vector
r_α	= radius of gyration, nondimensionalized with respect to semichord
s	= blade spacing (Fig. 1)
S_α	$= mbx_I$ = static mass moment per unit span about axis $x = ba$, positive when center of gravity (CG) is aft
t	= time
U	= freestream velocity relative to blades
U_F	= flutter speed
W	= work done by airstream on cascade, per cycle
x, y	= rectangular coordinates
$\bar{x}$	$= x/c$ = nondimensional x coordinate
x_I	= CG-EA offset, nondimensionalized with respect to semichord, positive when CG is aft
α	= torsional deflection, positive clockwise (Fig. 2)
γ_ω	$= \omega_B/\omega_T$ = frequency ratio, bending to torsion
δ	= logarithmic decrement (damping)
θ	= stagger angle (Fig. 1)
λ	= complex eigenvalue defined by Eq. (15)
μ	$= m/\pi\rho b^2$ = mass ratio of blade
ρ	= air density
σ	= interblade phase angle
ϕ	= phase angle between bending and torsion
ω	= frequency in rad/s
$\bar{\omega}$	$= \omega/\omega_T$ = nondimensionalized frequency
ω_B, ω_T	= uncoupled natural frequencies in bending and torsion, respectively
Ω_R	= rotational speed in rad/s
$[\,], \{\,\}$	= matrices
$\{\dot{}\}$	= differentiation with respect to time
$(\,)_0$	= complex amplitude of harmonic variable, e.g., $h = h_0 e^{i\omega t}$
$[\,]^{-1}$	= inverse of a matrix
$(\,)^R, (\,)^I$	= real and imaginary parts, respectively

Received Feb. 17, 1979; presented as Paper 79-0793 at AIAA/ASME/ASCE/AHS 20th Structures, Structural Dynamics, and Materials Conference, St. Louis, Mo., April 4-6, 1979; revision received July 20, 1979.

Index categories: Structural Dynamics; Airbreathing Propulsion; Rotating Machinery.

*Doctoral Candidate, Mechanics and Structures Dept., also, Director of Project Engineering, Pacific Airmotive Corp., Burbank, Calif. Member AIAA.

†Associate Professor of Engineering and Applied Science, Mechanics and Structures Dept. Associate Fellow AIAA.

I. Introduction

DESPITE a considerable research effort in the area of turbomachinery aeroelasticity over the past thirty years, flutter instabilites are still occurring in current technology engines[1,2] and research fans.[3] Once encountered, these instabilities have often proved very troublesome to eliminate,[4,5] requiring costly and time-consuming testing and redesign efforts.

Early studies of turbomachinery flutter emphasized the empirical approach. This was due partly to the fact that the necessary unsteady aerodynamic theories for cascades were not yet developed, and partly because it was believed that stall and choke types of flutter were the only ones possible. This conclusion was reached both by Pearson[6] and Schnittger[7] based on calculations using Theodorsen's isolated wing aerodynamics. When such calculations were applied to the engines at that time (around 1950), they indicated that classical bending-torsion flutter would require unreasonably high velocities and, therefore, this problem was not considered to be significiant from a practical point of view.

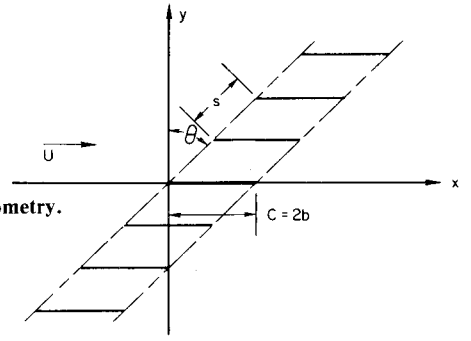

Fig. 1 Cascade geometry.

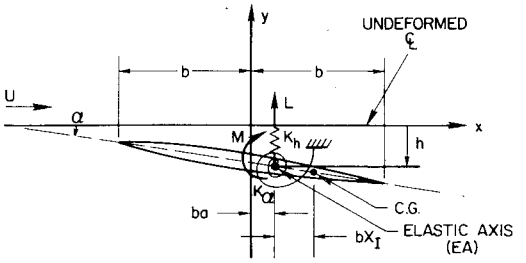

Fig. 2 Blade geometry and structural model.

Around 1960 it was generally accepted that cascade flutter is essentially a single-degree-of-freedom (SDOF) phenomenon—an assumption that is still in widespread use today. Since the possibility of SDOF torsional or bending flutter can be deduced directly from the aerodynamic coefficients, a considerable effort has been directed toward establishing unsteady aerodynamic theories for the various operating regimes of fans and compressors.

The purpose of this paper is to examine the effect of coupling between bending and torsion on the stability boundary of a typical cascade. It will be shown that the introduction of the bending degree of freedom has a pronounced effect on the flutter speed, despite the fact that there is no significant tendency for the bending and torsional frequencies to coalesce as flutter is approached.

Except for a paper by Carta[8] on coupled blade-disk-shroud flutter, the coupled bending-torsion problem for cascades has received little or no attention in the published literature. No results have previously been published comparing the SDOF vs the coupled bending-torsion stability boundaries. It should also be pointed out that Carta used Theodorsen's isolated wing aerodynamics, and his approach in determining the stability boundaries differs fundamentally from the method used in this paper.

II. Formulation of the Problem

A. Basic Assumptions

As is customarily done, the real rotor is modeled as an infinite two-dimensional cascade of identical flat airfoils in a uniform upstream flow, as shown in Fig. 1. The usual small-disturbance assumptions are used to linearize the problem about the zero deflection position, permitting the effects of thickness, camber, and mean angle of attack to be evaluated separately and superimposed. Only the effects due to the motion of the blades will be considered here. The cascade is, therefore, replaced by flat plates aligned with the undisturbed flow, and the linearized boundary conditions are satisfied on the mean position of the blades and their wakes. It will be assumed that all airfoils execute identical harmonic motion, with an arbitrary but constant phase angle σ between adjacent blades. The phase angle σ is restricted to the N discrete values $\sigma = 2\pi n/N;\ n = 0,1,2,\ldots,N-1$, where N is the number of blades in the rotor. This assumption is justified by Lane.[9] It should be noted, however, that more complicated mode shapes can occur under certain circumstances where Lane's assumptions no longer hold. One such case occurs when the inertia of the rotor must be considered finite, and torsional or lateral motion of the rotor has to be taken into account. Lane did show[9] that under certain conditions the mode shapes will still be of the simple form assumed earlier, even if torsional motion of the rotor is accounted for. A second, and possibly more important case, arises due to the fact that real rotors are "mistuned"; the blades have small differences in natural frequencies and mode shapes due to inherent manufacturing tolerances. It is well known that this leads to dynamic mode shapes where both amplitudes and phase angles vary from blade to blade.[10,11] Whitehead[12,13] concludes that mistuning is always beneficial in the flutter case, while a Russian paper[14] indicates the opposite to be true. The disagreement here is believed to be due to Whitehead's assumption that the interblade phase angle remains constant, even in the mistuned case. In fact, the latter paper, Ref. 14, suggests that mistuning sets up "exciters"—blades which extract energy from the airstream—while other blades become "dampers." Stability of the rotor is governed by the ratio of exciters to dampers, and the individual blade amplitudes and phase angles are found to vary considerably.

Since the main purpose of this paper is to investigate the basic nature of the coupled bending-torsion problem, these additional complications will not be considered and Lane's assumption about the flutter mode shapes will be used. Furthermore, due to the basic nature of this study, relatively simple structural and aerodynamic models, described later, are used.

B. Structural Model

The blades are modeled as "equivalent sections," as shown in Fig. 2, where the bending stiffness and torsional rigidity are represented by springs of stiffnesses K_h and K_α, respectively. Geometric and inertial properties of the blades are represented by their respective values at the three-quarters station of blade span, and the aerodynamic operating conditions are taken at the same location.

The coupled bending-torsion equations of motion for the nonrotating section are:

$$m\ddot{h} + S_\alpha \ddot{\alpha} + K_h h = -L \tag{1}$$

$$S_\alpha \ddot{h} + I_\alpha \ddot{\alpha} + K_\alpha \alpha = M \tag{2}$$

or, in matrix form,

$$[M]\{\ddot{q}\} + [K]\{q\} = \{F\} \tag{3}$$

where the mass matrix $[M]$, stiffness matrix $[K]$, generalized coordinates $\{q\}$; and force $\{F\}$, are given by

$$[M] = \begin{bmatrix} m & S_\alpha \\ S_\alpha & I_\alpha \end{bmatrix} \tag{4a}$$

$$[K] = \begin{bmatrix} K_h & 0 \\ 0 & K_\alpha \end{bmatrix} = \begin{bmatrix} m\omega_B^2 & 0 \\ 0 & I_\alpha \omega_T^2 \end{bmatrix} \tag{4b}$$

$$\{q\} = \begin{Bmatrix} h \\ \alpha \end{Bmatrix} \text{ and } \{F\} = \begin{Bmatrix} -L \\ M \end{Bmatrix} \tag{4c}$$

and the lift L and moment M, per unit span, are referred to the elastic axis (EA) located a distance ba behind midchord. The uncoupled natural frequencies

$$\omega_B = \sqrt{K_h/m} \text{ and } \omega_T = \sqrt{K_\alpha/I_\alpha}$$

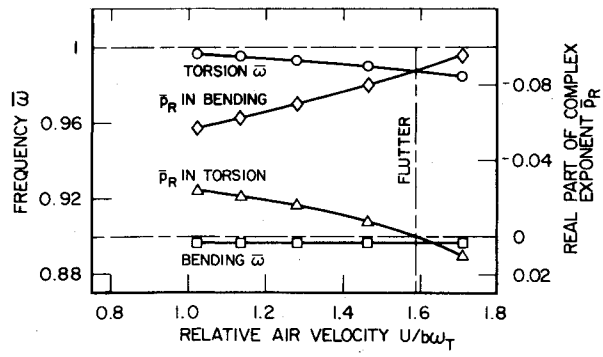

Fig. 3 Frequency and damping in bending and torsion vs airspeed ($\theta=60$ deg, $s/c=1.0$, $\mu=200$, $a=0$, $\gamma_\omega=0.9$, $r_\alpha^2=1/3$, $x_I=0.02$, $N=40$, and $g_B=g_T=0.005$).

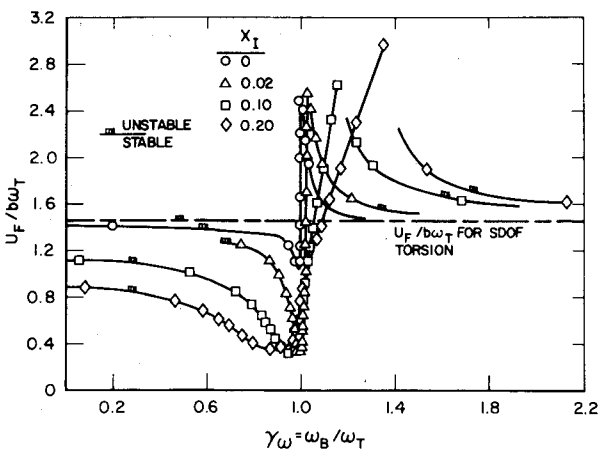

Fig. 4 Effect of offset between elastic axis (EA) and cross-sectional center of mass on flutter boundaries for EA at midchord and no structural damping ($\theta=60$ deg, $s/c=1.0$, $\mu=200$, $a=0$, $N=40$, $r_\alpha^2=1/3$, and $g_B=g_T=0$).

in bending and torsion are introduced for convenience. It will be assumed that the system executes simple harmonic motion, i.e.,

$$\{q\}=\begin{Bmatrix} h_0 \\ \alpha_0 \end{Bmatrix} e^{i\omega t}=\{q_0\}e^{i\omega t} \tag{5}$$

where the amplitudes h_0 and α_0 are assumed complex, to take care of any phase difference between bending and torsion. Substituting into Eq. (3), one obtains

$$(-\omega^2[M]+[K])\{q\}=\{F\} \tag{6}$$

Next, the aerodynamic forces are written in terms of nondimensionalized coefficients as follows:

$$L=L_0e^{i\omega t}=-\pi\rho b^3\omega^2[A_{11}(h/b)+A_{12}\alpha] \tag{7}$$

$$M=M_0e^{i\omega t}=\pi\rho b^4\omega^2[A_{21}(h/b)+A_{22}\alpha] \tag{8}$$

Substituting Eqs. (7) and (8) into Eq. (6), and dividing the first row by $\pi\rho b^3\omega^2$ and the second row by $\pi\rho b^4\omega^2$, yields the nondimensional flutter equations in matrix form

$$[S]\{\bar{q}\}=-[A]\{\bar{q}\} \tag{9}$$

where

$$\{\bar{q}\}=\begin{Bmatrix} h_0/b \\ \alpha_0 \end{Bmatrix}e^{i\omega t}=\begin{Bmatrix} \bar{h}_0 \\ \alpha_0 \end{Bmatrix}e^{i\omega t} \tag{10}$$

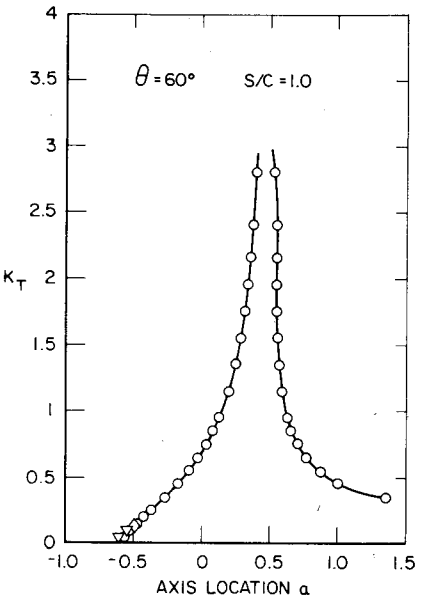

Fig. 5 Effect of EA location on SDOF torsional flutter ($N=40$, $g_T=0$).

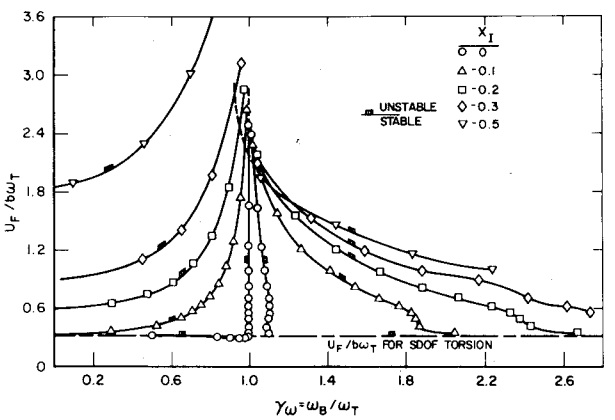

Fig. 6 Coupled bending-torsion flutter boundaries for EA at 3/4-chord and no structural damping ($\theta=60$ deg, $s/c=1.0$, $\mu=200$, $a=0.50$, $N=40$, $r_\alpha^2=0.5833$, and $g_B=g_T=0$).

are nondimensional generalized coordinates, and

$$[S]=\mu\begin{bmatrix} 1 & x_I \\ x_I & r_\alpha^2 \end{bmatrix}-(\mu/\bar{\omega}^2)\begin{bmatrix} \gamma_\omega^2 & 0 \\ 0 & r_\alpha^2 \end{bmatrix}$$

$$=[\bar{M}]-(1/\omega^2)[\bar{K}] \tag{11}$$

The matrices $[\bar{M}]$ and $[\bar{K}]$ are nondimensionalized mass and stiffness matrices, respectively, and the elements of the aerodynamic matrix $[A]$ are the nondimensional coefficients A_{ij} defined in Eqs. (7) and (8).

Structural damping is conveniently introduced in the equations of motion by multiplying the stiffness coefficients in bending and torsion by $(1+ig_B)$ and $(1+ig_T)$, respectively. This modifies the matrix $[S]$ in Eq. (11) as follows:

$$[S]=[\bar{M}]-(1/\bar{\omega}^2)[\bar{K}_d] \tag{12}$$

where

$$[\bar{K}_d]=\mu\begin{bmatrix} (1+ig_B)\gamma_\omega^2 & 0 \\ 0 & (1+ig_T)r_\alpha^2 \end{bmatrix} \tag{13}$$

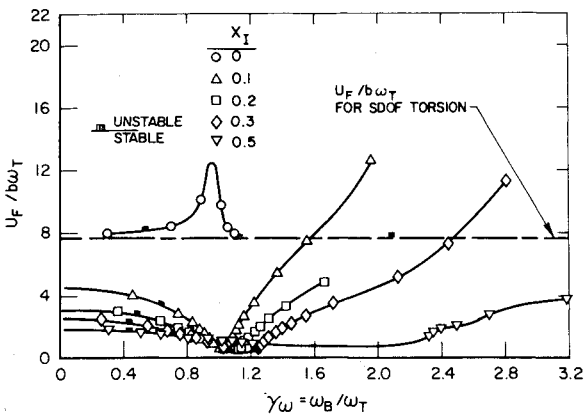

Fig. 7 Coupled bending-torsion flutter boundaries for EA at ¼-chord and no structural damping ($\theta = 60$ deg, $s/c = 1.0$, $\mu = 200$, $a = -0.50$, $N = 40$, $r_\alpha^2 = 0.5833$, and $g_B = g_T = 0$).

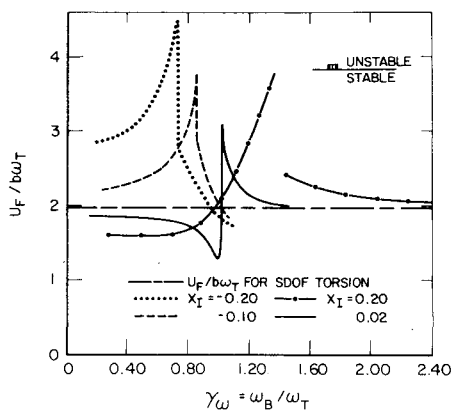

Fig. 8 Effect of structural damping on flutter boundaries for EA at midchord ($\theta = 60$ deg, $s/c = 1.0$, $\mu = 200$, $a = 0$, $N = 40$, $r_\alpha^2 = \frac{1}{3}$, and $g_B = g_T = 0.005$).

The structural damping g is related to the logarithmic decrement δ by $\delta \cong \pi g$, for small g. Substituting into Eq. (9) and rearranging yields

$$([\bar{M}] + [A])\{\bar{q}\} = (1/\bar{\omega}^2)[\bar{K}_d]\{\bar{q}\} \tag{14}$$

Multiplying both sides by $[\bar{K}_d]^{-1}$, we arrive at the eigenvalue problem in standard form,

$$[D]\{\bar{q}\} = \lambda\{\bar{q}\} \tag{15}$$

where $\lambda = 1/\bar{\omega}^2$ and the matrix $[D]$ is given by

$$[D] = [\bar{K}_d]^{-1}([\bar{M}] + [A])$$

$$= \begin{bmatrix} \dfrac{(\mu + A_{11})}{\gamma_\omega^2(1 + ig_B)} & \dfrac{(\mu x_I + A_{12})}{\gamma_\omega^2(1 + ig_B)} \\ \dfrac{(\mu x_I + A_{21})}{r_\alpha^2(1 + ig_T)} & \dfrac{(r_\alpha^2 + A_{22})}{r_\alpha^2(1 + ig_T)} \end{bmatrix} \tag{16}$$

In the analysis to follow, it should be kept in mind that, since the airloads were derived only for harmonic motion, the same restrictions also apply to Eq. (15). This implies that $\bar{\omega}$, and hence, λ, are real; such cases correspond to neutral stability, that is, the flutter boundary. Since $[D]$ is complex, but not Hermitian, it follows that the eigenvalue problem, in general, will have complex eigenvalues, implying the possibility of both damped (stable) and undamped (unstable) motion.

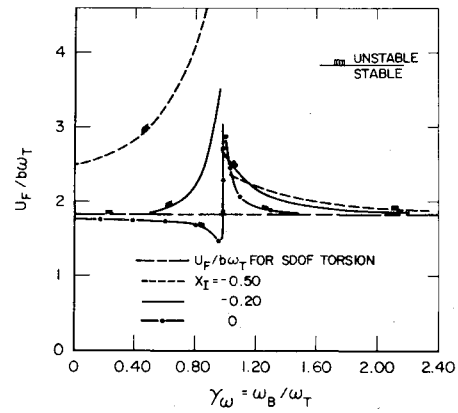

Fig. 9 Effect of structural damping on flutter boundaries for EA at ¾-chord ($\theta = 60$ deg, $s/c = 1.0$, $\mu = 200$, $a = 0.50$, $N = 40$, $r_\alpha^2 = 0.5833$, and $g_B = g_T = 0.005$).

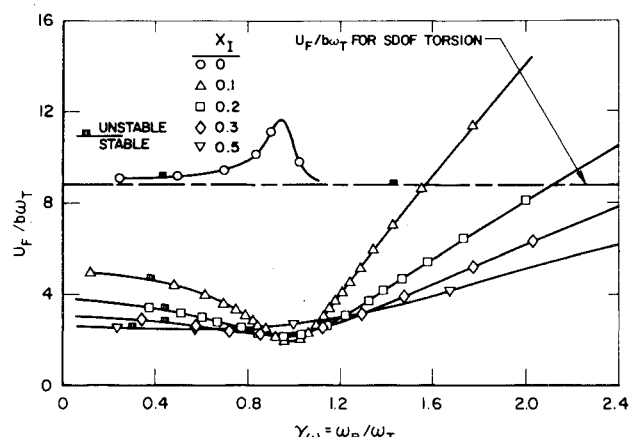

Fig. 10 Effect of structural damping on flutter boundaries for EA at ¼-chord ($\theta_0 = 60$ deg, $s/c = 1.0$, $\mu = 200$, $a = -0.50$, $N = 40$, $r_\alpha^2 = 0.5833$, and $g_B = g_T = 0.005$).

Before attempting to solve this system, it is instructive to consider the main features of the model and how effectively it can be expected to represent an actual rotor, particularly the coupled aspect of the problem. Coupling between bending and torsion in a rotor can take three forms: 1) structural coupling, due to pretwist, partspan shrouds, and disk interactions; 2) inertial coupling, due to static unbalance about the elastic axis, centrifugal effects, Coriolis forces, etc.; and 3) aerodynamic coupling, due to the nondiagonal form of the aerodynamic matrix.

The structural coupling will be particularly strong in shrouded fan rotors, but is also believed significant in nonshrouded rotors due to the high pretwist found in fan blades. The chief contributor to inertial coupling is the offset between the cross-sectional center of gravity and the elastic axis (CG-EA offset), which in rotating structures contributes an additional coupling term proportional to Ω_R^2, often referred to as the propeller moment. For rotors operating at high rotational speeds, Coriolis forces may also be important. Finally, the aerodynamic coupling is always present, except possibly for discrete combinations of reduced frequency and blade parameters. It will remain even after a transformation to normal coordinates, since the normal modes of the system will not, in general, diagonalize the aerodynamic matrix.

In the present paper, structural and inertial coupling strengths are modeled, or lumped through an "effective" static unbalance, or CG-EA offset x_I. The aerodynamic coupling is accounted for by including the off-diagonal terms A_{12} and A_{21}, in the aerodynamic matrix, consistent with the

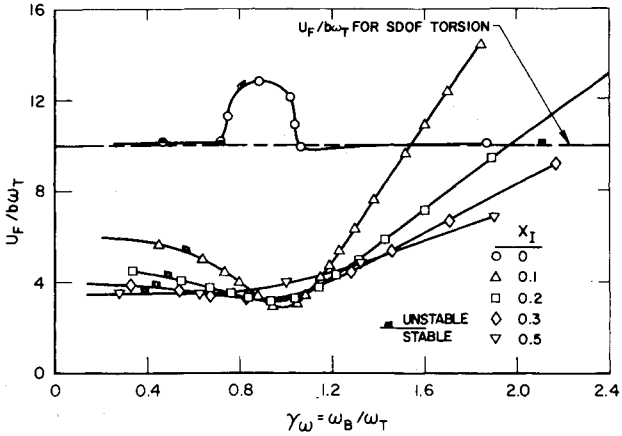

Fig. 11 Effect of strong structural damping on flutter boundaries for EA at ¼-chord ($\theta = 60$ deg, $s/c = 1.0$, $\mu = 200$, $a = -0.50$, $N = 40$, $r_\alpha^2 = 0.5833$, and $g_B = g_T = 0.02$).

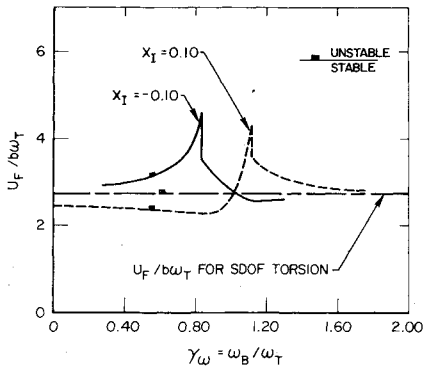

Fig. 12 Changeover in flutter mode from torsion to bending for $x_I = -0.10$ at $\gamma_\omega \simeq 0.835$ and from bending to torsion for $x_I = 0.10$ at $\gamma_\omega \simeq 1.12$ ($\theta = 60$ deg, $s/c = 1.0$, $\mu = 200$, $a = 0$, $N = 40$, $r_\alpha^2 = \frac{1}{3}$, and $g_B = g_T = 0.02$).

structural model used. The question naturally arises as to what justification one has for using x_I to model not only the inertial but also the structural coupling in real rotors.

First, it should be realized that the equations of motion, as expressed by Eq. (3), can be considered quite general. In fact, regardless of whether a finite-element model or a form of distributed coordinates, such as those employed in a Galerkin procedure, is used to model the blades, the final step in going back to the global coordinates $\{q\}$ will always lead to a matrix equation of the same basic form as Eq. (3). The stiffness matrix, however, will not necessarily be diagonal, indicating structural coupling between the degrees of freedom. Upon assuming simple harmonic motion, $\{q\} = \{q_0\}e^{i\omega t}$, one finds that the inertial and structural coupling terms, represented by the off-diagonal terms in the mass and stiffness matrices, enter the final eigenvalue problem, Eq. (15), in exactly the same form, now represented by off-diagonal terms in the matrix $[D]$. It, therefore, appears reasonable in this study to group the inertial and structural coupling and model their total strength through some effective GG-EA offset x_I.

The preceding arguments are easily generalized to an n-degree-of-freedom linear system, including the effects due to rotation. Inclusion of rotational effects offers no conceptual difficulties; their main effect on the system is to contribute certain additional terms in the stiffness matrix, thus raising the natural frequencies. Rotation also induces additional inertial coupling terms between the degrees of freedom.

In this paper, the rotational effects are incorporated by taking the appropriate natural bending and torsional frequencies for the rotating system. The coupling strength x_I is variable and considered symmetric between the two degrees of freedom. The aerodynamic coupling terms A_{12} and A_{21} are not equal, however, due to the basic nonconservative nature of the aerodynamic forces.

C. Unsteady Aerodynamics

The aerodynamic loads were evaluated using Whitehead's[15] solution for incompressible unsteady flow through a cascade, which was felt appropriate in view of the basic objective of this study. It should be pointed out that no results have previously been published for the coupled problem using an unsteady aerodynamic theory for cascades, since Carta's paper[8] used Theodorsen's isolated wing theory. Additional details on the unsteady aerodynamics can be found in Refs. 15 and 28.

A computer program has been written to evaluate the force and moment coefficients for given values of θ, s/c, k, and σ. The correctness of this program was checked by comparison to Whitehead's published results for six collocation points over a wide range of cascade parameters. Excellent agreement was obtained to within the four-decimal-place accuracy of Whitehead's results.

III. Method of Solution

The aeroelastic stability boundaries are obtained by solving a complex eigenvalue problem, Eq. (15), analogous to the isolated wing case.[16] The main difference from a computational standpoint is that the unsteady airloads are now dependent both on the reduced frequency k and the interblade phase angle σ. This means that there are two parameters in the eigenvalue problem, and it becomes necessary to determine the critical value of σ in addition to the flutter speed. This is accomplished by using the procedure suggested by Lane,[9] where the critical value of σ is determined by minimizing the flutter velocity with respect to σ, while restricting σ to the admissible values $\sigma = 2\pi n/N$; $n = 0,1,2,\ldots,N-1$.

To systematically investigate cascade stability over a wide range of design parameters, a computer program has been written, including the effect of structural damping. The eigenvalue problem given by Eq. (15) is solved directly, and from the two complex eigenvalues, λ_1 and λ_2, the two roots which are related to the exponent p of the time dependence e^{pt} (previously assumed harmonic $= e^{i\omega t}$) are obtained as follows:

$$p = (i/\sqrt{\lambda})\,\omega_T \tag{17}$$

or, in nondimensional form,

$$\bar{p} = p/\omega_T = \bar{p}_R + i\bar{\omega} \tag{18}$$

Instability occurs when $\bar{p}_R > 0$.

For the purpose of generating stability boundaries over a wide range of design parameters, it was found computationally efficient to proceed as follows:

1) Specify θ, s/c, and k.

2) Set up a loop to calculate airloads for each admissible $\sigma = 2\pi n/N$, $n = 0,1,\ldots,N-1$, and within this loop solve the eigenvalue problem for the desired range of coupling strengths and frequency ratios, $\gamma_\omega = \omega_B/\omega_T$. Check $\bar{p}_R$ for both roots. If $\bar{p}_R > 0$, return to the previous γ_ω and use the method of *regula falsi* to locate the exact flutter boundary $\gamma_{\omega F}$. Note that this iteration does not involve recalculation of airloads, and is, therefore, relatively fast.

3) After σ is cycled through all desired values, return to step 1, increment k, and repeat the procedure.

In generating the results for this paper, six-point collocation was used in calculating the aerodynamic matrix. Execution time to calculate the airloads and to solve the eigenvalue problem for a given set of k, σ, x_I, over a range of 24 values of γ_ω is about 0.2 s on the UCLA IBM 360/91 computer, including iteration at the flutter boundaries.

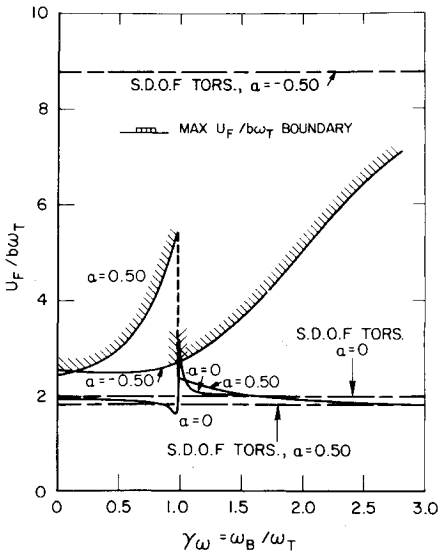

Fig. 13 Solution to design example (optimum EA location).

It should be pointed out that the method of solution presented here differs from the previously published method by Carta,[8] since the latter does not involve the solution of an eigenvalue problem. Essentially, Carta uses a single-degree-of-freedom analysis based on the system mode shapes in vacuum. Stability is determined from energy considerations identical to those used earlier by Greidanus[17] in studying low-speed flutter. More general stability criteria, based on energy considerations, were later given by Crisp.[18]

The results presented in this paper indicate that the coupled bending-torsion system should be used in a cascade flutter analysis; therefore, kinematic approaches of the type used by Carta, which constrain the mechanism of instability, may not give conservative results for a multi-degree-of-freedom system. This is not surprising in view of other analogous cases involving nonconservative systems.[19]

The correctness of the flutter boundaries obtained in this paper was checked by considering the energy exchange between the cascade and the surrounding airstream. The total work done by the airstream on the cascade, per cycle, is given by:

$$W = N\pi^2 \rho b^4 \omega^2 \cdot \{A_{11}^I \bar{h}_0^2 + [(A_{12}^I + A_{21}^I)\cos\phi - (A_{12}^R - A_{21}^R)\sin\phi]\bar{h}_0\alpha_0 + A_{22}^I \alpha_0^2\} \tag{19}$$

where ϕ is the phase angle by which torsion lags bending. When differences in notation are accounted for, this is exactly the same expression as obtained by Carta in Ref. 8. The flutter boundaries, obtained by solving the complex eigenvalue problem, Eq. (15), were checked by substituting the corresponding flutter mode shape $\bar{h}_0/\alpha_0$ and ϕ into Eq. (19) and verifying that $W=0$ on the boundary. Excellent agreement was obtained in all cases checked.

It is clear from Eq. (19) that, if the flutter mode shapes $\{\bar{h}_0/\alpha_0;\phi\}$ can be assumed known *a priori,* Carta's method will yield the same flutter boundaries as obtained by the solution of the eigenvalue problem, Eq. (15). It may be argued that for shrouded blades and blades mounted on relatively flexible disks, the flutter mode shape $\bar{h}_0/\alpha_0$ and phase angle ϕ should be strongly influenced by the natural modes in vacuum of the overall blade-shroud-disk system, and should, therefore, not change significantly as flutter is approached. To check this assumption, the behavior of the system mode shapes was studied for various levels of coupling strengths x_I as the flutter boundary was approached. As discussed under the structural model earlier, a large x_I can also be interpreted as representing strong structural coupling, i.e., a shrouded disk. Indeed, it was found that as x_I increased, the difference between the flutter mode shapes and the free vibration mode shapes in vacuum were found to decrease, and in some cases, were found to be negligible. However, this behavior was not found to be generally true; indeed, for reduced frequencies around 0.5 and less, the effects of the airloads on the mode shapes were no longer negligible, regardless of coupling strength. The change in mode shapes for strong coupling (x_I large) was usually most pronounced in the ratio $\bar{h}_0/\alpha_0$, the phase angle ϕ often remaining within ± 10 deg of the free mode phase angles (0 and 180 deg). For weak coupling strengths x_I, however, both $\bar{h}_0/\alpha_0$ and ϕ were found to change significantly as flutter was approached.

IV. Numerical Results

Some illustrative results are shown in Figs. 3-13. The numerical values of the design parameters are taken in the practical range of a current technology fan rotor: stagger angle $\theta = 60$ deg, spacing ratio $s/c = 1.0$, mass ratio $\mu = 200$ (titanium blades), and number of blades $N = 40$. The values of the other pertinent parameters are shown on the figures. In all of these examples, six-point collocation was used in calculating the unsteady aerodynamic forces.

Figure 3 shows the typical behavior of the frequency and damping in bending and torsion as flutter is approached. As can be seen, there is only a slight tendency toward frequency coalescence.

The significant effect that coupling between bending and torsion has on the nondimensionalized flutter speed $U_F/b\omega_T$, for the case of $a=0$ (EA at midchord) and no structural damping, is illustrated in Fig. 4. In Fig. 4, the coupling between the bending and torsional degrees of freedom is introduced by varying x_I, which represents the offset between the elastic axis and the cross-sectional center of mass of the blade. Thus, the bending and torsional degrees of freedom are coupled both dynamically (due to x_I) and aerodynamically through the appropriate unsteady aerodynamic coefficients. As indicated by the results shown in the figure, the inertial coupling between bending and torsion introduces very significant changes in the critical flutter speed $U_F/b\omega_T$ at which the blades can become unstable.

Figure 4 also reveals several interesting features of the coupled problem. First, a dip or "trench" is observed in all curves around frequency coincidence, $\gamma_\omega = \omega_B/\omega_T = 1$. This result can be anticipated from the analogous behavior for the case of an isolated wing. It is interesting to note that for this particular case ($a=0$, no damping), the minimum flutter speed $U_F/b\omega_T$ at the bottom of the trench is virtually independent of the coupling strength x_I, except for $x_I = 0$. Even a very weak coupling of $x_I = 0.02$, representing a CG-EA offset of only 1% of chord, produces a dip of about 20% when compared to the corresponding flutter speed for SDOF torsion. Increasing the coupling strength has the effect of widening the trench and moving it toward lower frequency ratios, γ_ω, for the case of positive x_I. To minimize confusion, no cases of negative coupling, $x_I < 0$, are shown in Fig. 4; such cases would appear roughly as a rotation of the corresponding curve for $x_I > 0$ about the line $\gamma_\omega = 1$.

Secondly, it is apparent from Fig. 4 that coupling between bending and torsion can also be beneficial, and actually raise the flutter speed above its corresponding SDOF torsional value. For EA at midchord, this was found to occur for all negative values of x_I over most of the range $0 < \omega_B/\omega_T < 1$. For positive x_I, roughly the opposite occurs: There is a rather steep wall around $\omega_B/\omega_T = 1$ where, as the frequency ratio is increased, the system stability increases at a very rapid rate, reaches a peak, and then drops asymptotically to the SDOF torsional value. This suggests the importance of considering the coupled problem when redesigning blades to alleviate a flutter problem.

It should be noted that the structural model used here accounts only for the fudamental bending and torsional

modes. Current technology fans often have second bending and first torsional frequencies close together, sometimes with frequency coincidence in the operating range.[5] To properly account for the interaction between these two modes, a more elaborate structural model with three degrees of freedom is needed. It is possible, however, that a qualitative feel for the result may be obtained by substituting the second bending frequency into $\gamma_\omega = \omega_B/\omega_T$ and use the simple two-degree-of-freedom model used in this paper. While $\gamma_\omega = \omega_B/\omega_T$ for first bending/first torsion is typically in the range 0.3-0.7, γ_ω for second bending/first torsion often fall in the dangerous range of 0.8-1.2.[1-3] It, therefore, appears that the interaction between the second bending and the first torsional modes may be potentially hazardous. Indeed, experimental evidence seems to support this, and rotors where the second bending and first torsional modes have had an actual or near-frequency coincidence have often encountered extremely troublesome flutter problems.[5]

It is known that the single-degree-of-freedom torsional flutter boundary predicted from Whitehead's incompressible cascade solution is very sensitive to the location of the torsional or elastic axis,[12] as shown in Fig. 5. The worst location is around ¾ chord ($a=0.50$), and the best location is close to ¼ chord ($a=-0.50$). Figures 6 and 7 illustrate the effect of location of the EA on the coupled bending-torsion case by showing what happens to the stability boundaries for axis locations at ¾ and ¼ chord, respectively. Here, the most striking effect due to the coupling between bending and torsion is observed. For the ¾ chord axis location ($a=0.50$), the introduction of the bending degree of freedom is strongly stabilizing, whereas, for the ¼ chord ($a=-0.50$) axis location, it is strongly destabilizing. For $a=0.50$, $x_I=-0.50$, and $\omega_B/\omega_T=0.75$, the coupled flutter speed is ten times higher than the corresponding SDOF torsional value. Similarly, Fig. 7 shows a drastic reduction in flutter speed, to less than 10% of the SDOF value when ω_B/ω_T is around one, and remaining less than 25% for ranges of ω_B/ω_T and x_I of a practical rotor. In the case $x_I=0$, corresponding to aerodynamic coupling only, both axis locations show stabilizing peaks around a frequency ratio of one.

In almost all of the cases, the critical phase angle σ for this 40-blade rotor was found to be $\sigma/2\pi=0.150$, or $\sigma=54$ deg. For $a=0$ (Fig. 4) and $x_I=0$, it was found that the critical value of σ changed around the bottom of the trench. For $\gamma_\omega<0.95$ and $\gamma_\omega>0.995$, the critical phase was $\sigma/2\pi=0.150$; whereas, in the range $0.95<\gamma_\omega<0.995$, the critical phase $\sigma/2\pi$ was found to take on the admissible values of 0.150, 0.175, 0.200, 0.225, 0.250, and back up to 0.150, with increasing γ_ω. This would indicate that for certain frequency ratios in this range, the flutter mode may be a superposition of two modes with different interblade phase σ. The theoretical possibility of such modes was discussed in detail by Lane,[9] while preliminary experimental evidence of their existence may be found in a paper by Stargardter.[20]

In some aeroelastic systems the instabilities are weak, such as the precone induced flap-lag instability of hingeless rotor blades, and can be easily eliminated by small amounts of structural damping.[27] Figures 8-10 show the stability boundaries in Figs. 4, 6, and 7, recomputed with structural damping $g_B=g_T=0.005$, corresponding to $\delta\simeq0.015$. Figure 8 should be compared to Fig. 4; Fig. 9 to Fig. 6; and Fig. 10 to Fig. 7, keeping in mind that the scale has changed on the $U_F/b\omega_T$ axis. As indicated by these results, addition of damping is stabilizing insofar as it reduces somewhat the unstable regions in the cases considered; however, it does not eliminate the instabilities. One can, therefore, conclude that the instabilities are physically significant. Again, the differences between the SDOF torsional and the coupled bending-torsion stability boundaries are quite pronounced.

Figure 11 illustrates the effect of very strong structural damping, $g_B=g_T=0.02$ ($\delta\simeq0.063$, or 6.3% of critical), for the case of EA at ¼ chord. The pronounced difference between the SDOF and the coupled flutter boundaries are seen to persist even in the presence of strong damping. In fact, the peak around $\omega_B/\omega_T=1$ for the case of aerodynamic coupling only, has now grown in width to a "bubble." Calculations with strong damping were also carried out for midchord and ¾-chord axis locations; these results also indicate that increased structural damping does not qualitatively affect the preceding conclusions.

Although there is experimental evidence that bending flutter can occur in cascades, it cannot be explained theoretically as an SDOF phenomenon, unless finite mean lift (or incidence) is accounted for.[13,21] This appears to be the case for both incompressible,[15] and compressible subsonic,[22] and supersonic[23-25] flows, although in the last case, strong shocks in the blade passages may also produce bending flutter.[26] However, the present study indicates that when coupling between bending and torsion is accounted for, the bending branch may actually become the unstable mode. Two typical cases are illustrated in Fig. 12. For the curve labeled $x_I=-0.10$, the flutter mode changes from torsion to bending at $\gamma_\omega\simeq0.835$. For the curve labeled $x_I=+0.10$, the flutter mode shape changes from bending to torsion around $\gamma_\omega\simeq1.12$. Similar cases of the bending branch becoming unstable were found to occur over a wide range of coupling strengths x_I. These changeovers manifest themeslves as discontinuities in the stability boundary when flutter speed $U_F/b\omega_T$ is plotted vs frequency ratio $\gamma_\omega=\omega_B/\omega_T$.

V. Design Example

Figure 13 illustrates the application of some of the preceding results to a simple design example. Consider a cascade of flat plate airfoils with the section parameters as shown below, and the CG fixed at midchord. Considering the effect of aerodynamic coupling and inertial coupling through CG-EA offset x_I and subject to the constraint $\omega_T=$const, which of the following three EA axis locations would give the highest flutter speed $U_F/b\omega$: ¼ chord, midchord, or ¾ chord? The problem may be thought of as simulating moving the EA position by moving the location of the part span shrouds along the blade chord, where the shrouds have been considered massless (inclusion of the shroud mass is straightforward). It also simulates the effect of hinge location on stability of movable guide vanes. Note that the solution, as shown in Fig. 13, is strikingly different from what would be predicted based on an SDOF torsion model alone.

Problem Statement

Flat plate cascade with section parameters: $\theta=60$ deg; $s/c=1.0$; $\mu=200$ (Ti); $N=40$; $r_\alpha^2=\frac{1}{3}$ about midchord; CG fixed at midchord; $g_B=g_T=0.005$ ($\delta\simeq0.015$). Given $\gamma_\omega=\omega_B/\omega_T$, what EA location maximizes $U_F/b\omega_T$: $a=0$, $a=0.50$, or $a=-0.50$?

Problem Solution:

From Fig. 13, the optimum axis location is:

$\gamma_\omega=\omega_B/\omega_T$	Optimum a
$\gamma_\omega<0.14$	-0.50 (¼ chord)
$0.14<\gamma_\omega<0.98$	$+0.50$ (¾ chord)
$0.98<\gamma_\omega<1.02$	0
$\gamma_\omega>1.02$	-0.50 (¼ chord)

VI. Conclusions

The major conclusions that can be drawn from this study are summarized below. They should be considered as indicative of trends, but must be interpreted in the light of the assumptions and models used in this study. The extension of this analysis to a more sophisticated structural model and appropriate aerodynamic theories for different speed regimes offers no conceptual difficulty, and such work is presently under way by the authors.

1) The effect of coupling between bending and torsion significantly changes the stability boundary of a typical cascade.

2) There is no appreciable tendency for the bending and torsional frequencies to coalesce as flutter is approached, except at very low reduced frequencies.

3) The location of the torsional axis has less of a drastic effect on the coupled problem than on the corresponding SDOF torsional problem.

4) Structural damping has a pronounced beneficial effect on the flutter boundaries.

5) Bending flutter is possible in the coupled case, even in the absence of finite mean lift or incidence.

References

[1] Jeffers, II, J. D. and Meece, Jr., C. E., "F100 Fan Stall Flutter Problem Review and Solution," *Journal of Aircraft*, Vol. 12, April 1975, pp. 350-357.

[2] Troha, W. and Swain, K., "Composite Inlays Increase Flutter Resistance of Turbine Engine Fan Blades," ASME Paper 76-GT-29, March 1976.

[3] Ware, T. C., Kobayashi, R. J., and Jackson, R. J., "High-Tip-Speed, Low-Loading Transonic Fan Stage," NASA CR-121263, 1974.

[4] Mikolajciak, A. A., Arnoldz, R. A., Snyder, L. E., and Stargardter, H., "Advances in Fan and Compressor Blade Flutter Analysis and Predictions," *Journal of Aircraft*, Vol. 12, April 1975, pp. 325-332.

[5] Goatham, J. I., "Design Considerations for Large Fan Blades," SAE Paper 690387, April 1969.

[6] Pearson, H., "The Aerodynamics of Compressor Blade Vibration," *Fourth Anglo-American Aeronautical Conference*, London, Sept. 1953, pp. 127-162.

[7] Schnittger, J. R., "Flutter Problems in Gas Turbines," in *Design and Performance of Gas Turbine Powerplants*, edited by W. R. Hawthorne and W. T. Olson, Princeton University Press, Princeton, N.J., 1960, pp. 425-459.

[8] Carta, F. O., "Coupled Blade-Disk-Shroud Flutter Instabilities in Turbojet Engine Rotors," *Journal of Engineering for Power*, 1967, pp. 419-426.

[9] Lane, F., "System Mode Shapes in the Flutter of Compressor Blade Rows," *Journal of the Aeronautical Sciences*, Vol. 23, Jan. 1956, pp. 54-66.

[10] Dye, R.C.F. and Henry, T. A., "Vibration Amplitudes of Compressor Blades Resulting from Scatter in Blade Natural frequencies," *Journal of Engineering for Power*, July 1969, pp. 182-188.

[11] El-Bayoumy, L. E. and Srinivasan, A. V., "Influence of Mistuning on Rotor-Blade Vibrations," *AIAA Journal*, Vol. 13, April 1975, pp. 460-464.

[12] Whitehead, D. S., "Torsional Flutter of Unstalled Cascade Blades at Zero Deflection," Great Britain A.R.C. R&M 3429, 1964.

[13] Whitehead, D. S., "Bending Flutter of Unstalled Cascade Blades at Finite Deflection," Great Britain A.R.C. R&M 3386, 1962.

[14] Movshovich, I. M., "Self-Induced Vibrations of Axial-Compressor Blades," *Transactions of the Moscow Aviation Institute*, No. 172, Moscow 1967. Translated in NASA TT F-547, "Investigation of Vibration and Stability of Aircraft Engine Components," edited by G. S. Skubachevskiy, Washington, D.C., 1969, pp. 71-82.

[15] Whitehead, D. S., "Force and Moment Coefficients for Vibrating Aerofoils in Cascade," Great Britain A.R.C. R&M 3254, 1960.

[16] Bisplinghoff, R. L., Ashley, H., and Halfman, R. L., *Aeroelasticity*, Addison-Wesley Publishing Company, Reading, Mass., 1955, pp. 532-568.

[17] Greidanus, J. H., "Low Speed Flutter," *Journal of the Aeronautical Sciences*, Vol. 16, 1949, pp. 127-128.

[18] Crisp, J.D.C., "The Equation of Energy Balance for Fluttering Systems with Some Applications in the Supersonic Regime," *Journal of the Aero/Space Sciences*, Vol. 26, Nov. 1959, pp. 703-716, 738.

[19] Bolotin, V. V., *Nonconservative Problems of the Theory of Elastic Stability*, The McMillan Company, New York, 1963.

[20] Stargardter, H., "Optical Determination of Rotating Fan Blade Deflections," ASME Paper 76-GT-48, 1976.

[21] Namba, M., "Subsonic Cascade Flutter with Finite Mean Lift," *AIAA Journal*, Vol. 13, May 1975, pp. 586-593.

[22] Whitehead, D. S., "Vibration and Sound Generation in a Cascade of Flat Plates in Subsonic Flow," Great Britain A.R.C. R&M 3685, 1970.

[23] Verdon, J. M. and McCune, J. E., "Unsteady Supersonic Cascade in Subsonic Axial Flow," *AIAA Journal*, Vol. 13, Feb. 1975, pp. 193-201.

[24] Verdon, J. M., "Further Developments in the Aerodynamic Analysis of Unsteady Supersonic Cascades," ASME Paper 77-GT-45, 1977.

[25] Kurosaka, M., "On the Unsteady Supersonic Cascade with a Subsonic Leading Edge—An Exact First-Order Theory—Part 2," *Journal of Engineering for Power, Transactions ASME*, Series A, Vol. 96, Jan. 1974, pp. 23-31.

[26] Goldstein, M. E., Braun, W., and Adamczyk, J. J., "Unsteady Flow in a Supersonic Cascade with Strong In-Passage Shocks," *Journal of Fluid Mechanics*, Vol. 83, Pt. 3, Nov. 1977, pp. 569-604.

[27] Friedmann, P., "Recent Developments in Rotary-Wing Aeroelasticity," *Journal of Aircraft*, Vol. 14, Nov. 1977, pp. 1027-1041.

[28] Bendiksen, O. and Friedmann, P., "Coupled Bending-Torsion Flutter in Cascades," AIAA Paper 79-0793, St. Louis, Mo., April 1979.